Supplementary Material

Combining microenvironment normalization strategies to improve cancer immunotherapy

Fotios Mpekris, Chrysovalantis Voutouri, James W. Baish, Lance L. Munn, Dan G. Duda, Triantafyllos Stylianopoulos, Rakesh K. Jain

Description of the mathematical model

Kinematics of tumor growth

The mathematical model accounts for the growth of a spherical tumor with initial diameter 500 μm surrounded by normal tissue. Tumor growth is modeled based on the multiplicative decomposition of the deformation gradient tensor (**F**), which describes the kinematics of the tumor. The kinematics of the tumor are decomposed into two components, the growth component ($\mathbf{F}_g$) which accounts for the growth of the tumor and the elastic component ($\mathbf{F}_e$) which accounts for mechanical interactions of the tumor with the surrounding normal tissue (1, 2),

$$\mathbf{F} = \mathbf{F}_e \mathbf{F}_g, \tag{1}$$

The growth component is set to be homogenous and isotropic (3, 4)

$$\mathbf{F}_g = \lambda_g \mathbf{I}, \tag{2}$$

where λ_g is the growth stretch ratio, which describes the growth of cancer cells and cancer stem cells (proliferation minus apoptosis). The elastic component $\mathbf{F}_e$ of the deformation gradient tensor is determined from Eq. (1) as

$$\mathbf{F}_e = \mathbf{F}\,\mathbf{F}_g^{-1}. \tag{3}$$

Calculation of the growth stretch ratio λ_g

The growth stretch ratio is calculated taking into account the proliferation of three types of cancer cells, namely non-stem cancer cell (CC), stem-cell-like cancer cell (CSC) and induced cancer cells (ICC) (3, 5-7). In particular, we used the expression

www.pnas.org/cgi/doi/10.1073/pnas.1919764117

$$\frac{d\lambda_g}{dt} = \frac{1}{3}\left(\frac{T}{T_{tot}} S_T^c + \frac{C_{sc}}{T_{tot}} S_{C_{sc}}^c + \frac{I}{T_{tot}} S_I^c\right)\lambda_g , \tag{4}$$

where T is the CC population, C_{sc} is the CSC population, I is the ICC population, T_{tot} is the total density of cells given by the sum of the three populations, and S_T^c, S_{Csc}^c and S_I^c are the proliferation/degradation rates of CCs, CSCs and ICCs, respectively (given below in Eq. (7)).

Tumor microenvironment components

In our model, we account for interactions among cancer cells, cancer stem cells, cells of the immune system and the tumor vasculature, which are described below.

Cancer cells

The population dynamics of non-stem cancer cells (CCs), stem-cell-like cancer cells (CSCs, which are resistant to drugs, hypoxia and immune system) and induced cancer cells (ICCs, CCs that are induced by chemotherapy to acquire a more stem-like phenotype) are described by (8-10):

$$\begin{aligned}
\frac{\partial T}{\partial t} &= \nabla\cdot(\mathrm{D}_{cell}\nabla T) + GT - cNT - D + p_{CT}C_{sc} + p_{IT}I - \left(p_{TC} + p_{TI}\right)T - \lambda_{M1}M_1T \\
\frac{\partial C_{sc}}{\partial t} &= \nabla\cdot(\mathrm{D}_{cell}\nabla C_{sc}) + \alpha_{\mathrm{csc}}GC_{sc} - c_{\mathrm{csc}}NC_{sc} - D_{\mathrm{csc}} + p_{TC}T + p_{IC}I - \left(p_{CT} + p_{CI}\right)C_{sc} , \\
\frac{\partial I}{\partial t} &= \nabla\cdot(\mathrm{D}_{cell}\nabla I) + \alpha_I GI - c_I NI - D_I + p_{TI}T + p_{CI}C_{sc} - \left(p_{IT} + p_{IC}\right)I
\end{aligned} \tag{5}$$

where T is the population of CCs, C_{sc} of CSCs, I of ICCs, N of NK cells, L of $CD8^+$ T-cells, M_1 of M1-like TAMs cells, D_{cell} is the cancer cell diffusion coefficient, c and D are the fractions of tumor cells killed by NK and $CD8^+$ T-cells, respectively. G describes the proliferation of CCs, CSCs and ICCs as a function of oxygen. For the coefficients of the proliferation rates of CSCs and ICCs, i.e., α_{csc} and α_I, respectively, we assume that for normal oxygen levels they are equal to one so that all cancer cell types have the same proliferation as that of CCs. In hypoxic conditions, however, the proliferation of cancer cells with a stem-like phenotype increases. Thus, we assume that their proliferation increases inversely proportional to the oxygen concentration so that as oxygen concentration approaches zero, the proliferation rates are twice as much as the rate in normal

oxygen (11). For the parameters c_{csc}, D_{csc}, c_I, and D_I that describe the killing potential of immune cells on CSCs and ICCs, we assume that they are more resistant in interactions with immune cells. According to experimental data (12), the cytotoxicity of $CD8^+$ T-cells against CSCs is taken to be 7-fold lower than that of CCs. As a result, the parameters that describe the killing of CSCs by immune cells are assumed to be the same as for the CCs but multiplied by a factor of 0.14. The rates of transfer of cancer cells from a type *i* to a type *j* are described by p_{ij} and their values were determined in (10). Additionally, the parameter λ_{M1} denotes the tumoricidal effect of M1-like TAMs in cancer cells according to Ref. (13).

The dependence of cancer cell proliferation on the local oxygen concentration, G, is assumed to follow Michaelis-Menten kinetics and has the form (14, 15):

$$G = \frac{k_1 c_{ox}}{k_2 + c_{ox}}, \tag{6}$$

where k_1 and k_2 are growth rate parameters and c_{ox} is the oxygen concentration.

The creation/degradation of the solid phase, S_T^c, S_{Csc}^c and S_I^c is expressed as (8):

$$\begin{aligned} S_T^c &= GT - cNT - D + p_{CT}C_{sc} + p_{IT}I - \left(p_{TC} + p_{TI}\right)T - \lambda_{M1}M_1T \\ S_{Csc}^c &= \alpha_{\mathrm{csc}}GC_{sc} - c_{\mathrm{csc}}NC_{sc} - D_{\mathrm{csc}} + p_{TC}T + p_{IC}I - \left(p_{CT} + p_{CI}\right)C_{sc} \\ S_I^c &= \alpha_I GI - c_I NI - D_I + p_{TI}T + p_{CI}C_{sc} - \left(p_{IT} + p_{IC}\right)I \end{aligned} \tag{7}$$

Immune cells

For the immune system, four key types of immune cells are considered in this model: natural killer (NK) cells, $CD8^+$ T-cells, and $CD4^+$ T-cells, including the regulatory T-cell (Treg) subset. Based on pertinent studies (9, 16, 17), the system of equations accounts for the recruitment rates of the immune cells, their inactivation by cancer cells, the inhibitory role of Tregs and M2-like TAMs as well as their death rate and interaction with cancer cells. [Please see the next section for TAMs.]

$$\frac{\partial N}{\partial t} = \sigma_{nk} - f_{NK}N + \frac{g_{NK}T^2}{h+T^2}N - p_{im}NT - \lambda_{reg}T_{reg}N - \lambda_{M2}M_2N$$
$$\frac{\partial L}{\partial t} = \sigma_{T8} - m_{T8}L + \frac{j_{T8}D^2}{k_{im}+D^2}L - qLT + (r_N N + r_{Cd4}C_{d4})T - \lambda_{reg}T_{reg}L - \lambda_{M2}M_2L$$
$$\frac{\partial C_{d4}}{\partial t} = s_{CD4} + re_{Cd4}C_{d4}\left(1 - \frac{C_{d4}}{C_{d4,\max}}\right) - \mu_{C_{d4}}C_{d4} \quad , \qquad (8)$$
$$\frac{\partial T_{reg}}{\partial t} = g_{reg}T_{reg} - m_{reg}T_{reg}$$

where C_{d4} is the population of $CD4^+$ T-cells and T_{reg} is the population of the Treg cells. Furthermore, f_{NK}, m_{T8} and m_{reg} are death rates of NK cells, $CD8^+$ T-cells and Treg cells respectively, g_{NK}, j_{T8} and g_{reg} are recruitment rates of immune cells, p_{im} and q are inactivation rates of immune cells by CCs, σ_{nk} and σ_{T8} are constant sources of NK and $CD8^+$ T-cells respectively, r_N is the rate at which tumor-specific $CD8^+$ T-cells are stimulated to be produced as a result of tumor cells killed by NK cells and λ_{reg} is the inhibition term of NK cells and $CD8^+$ T-cells from Treg cells. Under anoxic conditions we used the lowest value for the activity of NK cells and $CD8^+$ T-cells reported in de Pillis et al. (9), which increased linearly to the highest value for normal oxygen conditions. The values of f_{NK} and m_{T8} are modified to depend on oxygen levels. According to experimental data (18), a 40 times decrease in oxygen concentration (from 20% to 0.5%) doubled the apoptotic rate of immune cells. Additionally s_{CD4} is the source of $CD4^+$ T-cells, μ_{Cd4} is the natural death rate of $CD4^+$ T-cells, re_{Cd4} is the growth rate of $CD4^+$ T-cells and $C_{d4,max}$ is the maximum $CD4^+$ T-cells population (19, 20). r_{Cd4} is the stimulation rate of $CD8^+$ T-cells by $CD4^+$ T-cells as mentioned previously (21-23). The source term of $CD4^+$ T-cells s_{CD4} will depend on oxygen concentration, as according to previous studies under hypoxic conditions it decreased 8 times (24). Furthermore, a decrease of M2-like TAMs resulted in higher numbers of $CD8^+$ T-cells and NK cells, while $CD4^+$ T-cells were not affected according to experimental data (25) and these observations are described by the parameter λ_{M2}. The equations for populations of cells are rendered dimensionless by dividing the number of cells per finite element node by the initial number of cancer cells, $T_0=5\times10^2$ cells. The initial population of cancer cells was taken to be: 98% CCs, 1% CSCs and 1% ICCs (26).

The parameter D denotes the fractional cell kill of tumor cells by $CD8^+$ T-cells and given by equation (9, 27):

$$D = d_{im} \frac{\left(\frac{L}{T}\right)^{\lambda_{im}}}{s + \left(\frac{L}{T}\right)^{\lambda_{im}}} T \,, \tag{9}$$

where d_{im} is the saturation level of fractional tumor cell kill by $CD8^+$ T-cells, s is steepness coefficient of the tumor-$CD8^+$ T-cells competition term and λ_{im} the exponent of fractional cell kill by $CD8^+$ T-cells.

Immunotherapy with anti-PD-1 is modeled as an increase in the source term of $CD8^+$ T-cells, σ_{T8} and with anti-CTLA-4 as an increase of death rate of Treg cells, m_{reg}.

Tumor Associated Macrophages (TAMs)

We account for two different types of TAMs, M1-like and M2-like:

$$\begin{aligned} \frac{\partial M_1}{\partial t} &= g_{m1} M_1 - m_{m1} M_1 \\ \frac{\partial M_2}{\partial t} &= g_{m2} M_2 - m_{m2} M_2 + r_{Cvegf,M2} C_{vegf} M_2 \end{aligned} \,, \tag{10}$$

g_{M1} and g_{M2} are the production rates of M1-like and M2-like TAMs, which depend on oxygen levels according to previous studies (25, 28, 29) showing that a decrease in hypoxia skewing TAM polarization away from the M2- to M1-like phenotype. According to previous studies TAMs are associated with VEGF expression (25, 30, 31). Specifically, VEGF-A overexpression correlated with higher numbers of M2-like TAMs ($r_{Cvegf,M2}$).

Biphasic formulation of the tumor's mechanical behavior

The mass balance equation for the fluid phase is (5, 7):

$$\frac{\partial \Phi^f}{\partial t} + \nabla \cdot (\mathbf{v}^f \Phi^f) = Q, \tag{11}$$

where Φ^f is the volume fraction of the fluid phase and $\mathbf{v}^f$ is the corresponding velocity. The sum of fluid and solid phase is equal to unity. Fluid velocity $\mathbf{v}^f$ is given by Darcy's law:

$$\mathbf{v}^f = \frac{-k_{th} \nabla p_i}{\Phi^f} + \mathbf{v}^s, \tag{12}$$

with k_{th} the hydraulic conductivity of the interstitial space and $\mathbf{v}^f$ is the velocity of solid phase.

The term Q in Eq. (11) denotes the fluid flux entering from the blood vessels into the tumor or the surrounding normal tissue minus the fluid flux exiting through lymphatic vessels, and is expressed as (4):

$$Q = L_p S_v (p_v - p_i) - L_{pl} S_{vl} (p_i - p_l), \tag{13}$$

where L_p, S_v and p_v are the hydraulic conductivity, vascular density and vascular pressure, respectively, L_{pl}, S_{vl} and p_l are the corresponding quantities for lymphatic vessels, and p_i is the interstitial fluid pressure.

According to the biphasic theory for soft tissues (32), the total stress tensor $\boldsymbol{\sigma}_{tot}$ is the sum of the fluid phase stress tensor $\boldsymbol{\sigma}^f = -p_i \mathbf{I}$ and the solid phase stress tensor $\boldsymbol{\sigma}^s$. As a result, the stress balance is written as:

$$\nabla \cdot \boldsymbol{\sigma}_{tot} = \mathbf{0} \Rightarrow \nabla \cdot (\boldsymbol{\sigma}^s - p_i \mathbf{I}) = \mathbf{0}, \tag{14}$$

where the Cauchy stress tensor of the solid phase $\boldsymbol{\sigma}^s$ is given by (33):

$$\boldsymbol{\sigma}^s = J_e^{-1} \mathbf{F}_e \frac{\partial W}{\partial \mathbf{F}_e^T}, \tag{15}$$

The tumor mechanical behavior was modeled to be incompressible and neo-Hookean with strain energy density given by (34-37):

$$W = \frac{\mu(-3 + II_1)}{2} - p\left(-1 + J_e + \frac{p}{2k}\right), \tag{16}$$

where μ and k are the shear and bulk modulus of the material, respectively, J_e is the determinant of the elastic deformation gradient tensor $\mathbf{F}_e$, $II_1 = I_1 J_e^{-2/3}$ where $I_1 = \mathrm{tr}\mathbf{C}_e$ is the first invariant of the

elastic Cauchy-Green deformation tensor $\mathbf{C}_e = \mathbf{F}_e^{\mathrm{T}} \mathbf{F}_e$, and p is a penalty variable introduced for near incompressible materials. The surrounding normal tissue was assumed to be compressible and neo-Hookean with a Poisson ratio of 0.2.

Functional vascular density

To quantify the functional vascular density, we assume that it is affected by the decrease in the vessel diameter (d/d_o) owing to the increased number of cancer cells (38) and the elevation of solid stress (39). Also the functional vascular density depends on the permeability of the tumor vessel wall (40) as hyper-permeable vessels reduce vessel perfusion and functionality.

The functional vascular density will be given from:

$$S_v = \frac{d}{d_0} S_v^0 \rho_v^{EC}, \tag{17}$$

where S_V^0 will depend on vessel wall pore size (i.e., permeability) and ρ_v^{EC} is the density of endothelial cells which is given below. Vessel wall pore size depends on IFNγ concentration as described below (page 11).

Oxygen Concentration

The rate of change of oxygen in the tumor tissue was taken to depend both on its transport through convection and diffusion, as well as the amount of oxygen consumed by cells, and the amount that enters the tissue from the blood vessels (3, 5), i.e.,

$$\frac{\partial c_{ox}}{\partial t} + \nabla \cdot \left(c_{ox} \mathbf{v}^f \right) = D_{ox} \nabla^2 c_{ox} - \frac{A_{ox} c_{ox}}{c_{ox} + k_{ox}} T_{tot} + P_{er} S_V \left(C_{iox} - c_{ox} \right), \tag{18}$$

where c_{ox} is the oxygen concentration, D_{ox} is the diffusion coefficient of oxygen in the interstitial space, A_{ox} and k_{ox} are oxygen uptake parameters, P_{er} is the vascular permeability of oxygen that describes diffusion across the tumor vessel wall and C_{iox} is the oxygen concentration in the vessels. The transvascular transport of oxygen was taken to be diffusion dominated given that convection is negligible for oxygen compared to diffusion (41). Given the uniform alleviation of the interstitial

fluid pressure in tumors, pressure gradients within the tissue and across the tumor vessel wall are small (42) and thus, Peclét numbers are expected to be low.

Tumor Vasculature Components

Endothelial cell transport equation

The flux of endothelial cell is given by the equation (43):

$$\frac{\partial \hat{e}}{\partial t} = \nabla \cdot (D_{EC}(a1, a2)\nabla \hat{e} - x_n \hat{e} H(1-\hat{e}) C^0_{vegf} \nabla \hat{C}_{vegf} - W_{Se} x_n \hat{e} H(1-\hat{e}) C^0_S \nabla \hat{C}_S) + \frac{1}{e_0}(\lambda_1 C^0_{vegf} e_0 \hat{C}_{vegf} \hat{e} + \lambda_2 C^0_{vegf} e_0 \hat{C}_{vegf} \hat{e}) H(1-\hat{e}) - (\lambda_3 e_0 \hat{e} + \lambda_4 e_0 \hat{e})\hat{e} - k^{ec}_{a-vegf} C_{vegf} \quad , \qquad (19)$$

Endothelial cell proliferation is based on VEGF and CXCL12 concentration as well as endothelial cell density. $\hat{e}$ is the dimensionless endothelial cell density. $\widehat{C_{vegf}}$ and C^0_{vegf} are dimensionless and reference VEGF concentrations. Endothelial cell diffusion coefficient depends on Ang1 and Ang2: $D_{EC}(a_1,a_2) = D_{ec}(1+ s_1a_1)^{-a}(1+ s_2a_2)^b$ with a and b to be unity (44). χ_n is a chemotactic term and W_{Se} is a weighting function describing the contribution of VEGF and CXCL12 on endothelial cell transport. The dimensionless concentration of the endothelial cells is calculated by division with the reference concentration $\hat{e} = \frac{e}{e_0}$. Loss terms describing killing of endothelial cells are also included. The parameters λ_1, λ_2, λ_3 and λ_4 are constant positive parameters. The parameter $k^{ec}_{a-vegf}$is a time and dose dependent parameter that describes the effect of anti-VEGF treatment on endothelial cells according to experimental studies (45, 46).

Pericytes transport equation

Two populations/phenotypes of pericytes are considered: pericytes that are tightly associated with endothelial cells and assumed to be immotile and pericytes that are dissociated from endothelial cells and can be motile. Production rates of both phenotypes depends on PDGF-B concentrations as well as on their own concentrations.

Immotile pericytes transport equation

The pericytes density is given by the equation (47, 48):

$$\frac{\partial p_{cim}}{\partial t} = \beta_{p_c} \frac{p_{cim}}{1+ p_c / p_c^0} \frac{p_b H(\lambda_{p_b} p_b - c_{p_b})}{p_b + \alpha_{p_{c1}}} - \mu_{p_c} \frac{a_2 H(a_2 - a_{p_{c3}})}{a_2 + a_{p_{c2}}} p_{cim} + \alpha_{p_{c4}} (p_{cim\max} - p_{cim}), \qquad (20)$$

where p_c is the total pericytes density (p_c=p_{cim}+p_{cm}), $p^0{}_c$ is the pericyte reference value, p_b is the PDGF-B concentration, p_{cimmax} is the carrying capacity of the immotile pericyte density, β_{pc}, λ_{pb}, c_{pb}, α_{p1}, α_{p2}, α_{p3}, α_{p4}, μ_{pc} are constant positive parameters.

Motile pericytes cells transport equation

The motile pericyte density is given by the equation (47, 48),

$$\frac{\partial p_{cm}}{\partial t} = \nabla \cdot (D_{p_c} \nabla p_{cm}) - \nabla \cdot (k_{p_c} p_{cm} \nabla p_b) - a_{p_{c4}} (p_{cim\max} - p_{cim}) + \beta_{pc} \frac{p_{cm}}{1+ p_c / p_c^0} \frac{p_b H(\lambda_{p_b} p_b - c_{p_b})}{p_b + \alpha_{p_{c1}}}$$
$$- \mu_{p_c} \frac{a_2 H(a_2 - a_{p_{c3}})}{a_2 + a_{p_{c2}}} p_{cm} - \mu_{p_{c2}} H(c_{pb} - \lambda_{p_b} p_b) p_{cm} \qquad (21)$$

where k_{pc} is a chemotactic constant, D_{pc} is the diffusion coefficient of motile pericytes and μ_{pc2} is a constant positive parameter.

VEGF transport equation

VEGF concentration is determined by diffusion, production from cancer cells under hypoxic conditions and binding to endothelial cells receptors (43). VEGF concentration is governed by the equation (43):

$$\frac{\partial \hat{C}_{vegf}}{\partial t} = \nabla \cdot (D_{VEGF} \nabla \hat{C}_{vegf}) + \frac{\lambda_{10}}{C_{vegf}^0} G_a(\hat{c}_{ox}) T - (\lambda_{11} e^0 \hat{e} + \lambda_{12} e_0 \hat{e}_0 + \lambda_{13}) \hat{C}_{vegf} - \lambda_{CD4,Cvegf} C_{d4} \hat{C}_{vegf} - k_{a-vegf}^{vegf} C_{vegf}, \qquad (22)$$

Where $\widehat{C_{vegf}}$ is the dimensionless VEGF concentration calculated with division with a reference value $\widehat{C_{vegf}} = \frac{C_{vegf}}{C_{vegf}^0}$ and $\widehat{c_{ox}}$ is the dimensionless oxygen concentration normalized as: $\widehat{C_{ox}} = \frac{C_{ox}}{C_{ox}^0}$.

VEGF is assumed to be produced by cancer cells only and its production is enhanced under hypoxic conditions as described by the oxygen tension term G_a(43).

$$G_a(\widehat{c_{ox}}) = \begin{cases} 3\widehat{c_{ox}} \text{ for } 0<\widehat{c_{ox}}<0.5 \text{ (hypoxia)} \\ 2 - \widehat{c_{ox}} \text{ for } 0.5<\widehat{c_{ox}}<1 \text{ (normoxia)} \\ \widehat{c_{ox}} \text{ for } 1<\widehat{c_{ox}} \text{ (hyperoxia)} \end{cases}$$

VEGF becomes unavailable due to binding to endothelial cells VEGF receptors and it can also diffuse in the tumor with a diffusion coefficient D_{VEGF} . λ_{10}, λ_{11}, λ_{12} and λ_{13} are positive constants. Additionally, knockout of $CD4^+$ T cells resulted in overexpression of VEGF ($\lambda_{CD4,Cvegf}$) and not significant differences in Ang1-Ang2 (21). The parameter $k_{a-vegf}^{vegf}$is a time and dose dependent parameter that describes the effect of anti-VEGF treatment on VEGF levels according to experimental studies (45, 46).

CXCL12 transport equation

The stromal cell derived factor 1 (SDF1α) is also known as C-X-C motif chemokine 12 (CXCL12). We suggest in the model that VEGF released by hypoxic cancer cells up-regulates CXCL12 from cancer cells and that CXCL12 is also produced by endothelial cells in a VEGF dependent manner (49). Therefore, CXCL12 is produced by both cancer cells and endothelial cells and it is also up-regulated by hypoxia and VEGF (49). The transport of CXCL12 is governed by:

$$\frac{\partial \hat{C}_S}{\partial t} = \frac{\lambda_{10}}{C_s^o} G_a(\hat{c}_{ox}) T + \frac{\lambda_{13}}{C_s^o} C_V^o \hat{C}_V H(1-\hat{e}) - \lambda_{13} \hat{C}_S \qquad (23)$$

where λ_{10}, and λ_{13} are positive parameters. The dimensionless CXCL12 concentration is given by division with a reference concentration $\widehat{C_s} = \frac{C_s}{C_S^0}$.

PDGF-B transport equation

PDGF-B was assumed to be produced by endothelial cells and binds to pericytes (50). PDGF-B concentration is governed by the equation (51):

$$\frac{\partial p_b}{\partial t} = D_{p_b}\nabla^2 p_b + \beta_{p_b}\hat{e} - \mu_{p_b} p_b - \gamma_{p_b} p_b p_c \tag{24}$$

where β_{pd}, μ_{pb} and γ_{pb} are positive parameters, D_{pb} is the PDGF-B diffusion coefficient.

Ang1 and Ang2 transport equations

Ang1 is assumed to be produced by pericytes and Ang2 by endothelial cells, respectively. Their production is enhanced by hypoxia based on VEGF levels (44). Angiopoietin 1(Ang1, α_1) and angiopoietin 2 (Ang2, α_2) are up-regulated by hypoxia and produced by endothelial cells.

$$\frac{\partial \hat{a}_1}{\partial t} = \frac{b_1}{a_0^1} p_c + \mu_1(1-\hat{a}_1) \tag{25}$$

$$\frac{\partial \hat{a}_2}{\partial t} = \frac{b_2}{a_2^1} G_a(\hat{c}_{ox})\hat{e}e_0 - \mu_2\hat{a}_2 \tag{26}$$

where b_1, b_2, m_1 and m_2 are positive constants. The dimensionless Ang1 and Ang2 are given by division with a reference concentration $\widehat{a_1} = \frac{a_1}{a_1^0}$, $\widehat{a_2} = \frac{a_2}{a_2^0}$. The oxygen tension term G_a is the same as used for VEGF and CXCL12. For the simplicity of the equations, we neglect diffusion of Ang1 and Ang2 and binding to specific Tie receptors (52, 53).

IFNγ transport equation

IFNγ concentration is determined by diffusion, production from $CD4^+$ T-cells and $CD8^+$ T-cells and degradation:

$$\frac{\partial IFN_\gamma}{\partial t} = \nabla.(D_{IFN\gamma}\nabla.IFN_\gamma) + \lambda_{production}^{IFN\gamma} IFN_\gamma - \lambda_{\deg radation}^{IFN\gamma} IFN_\gamma \tag{27}$$

where $D_{IFN\gamma}$ is the diffusion coefficient, $\lambda_{production}^{IFN\gamma}$ the production term and $\lambda_{\deg radation}^{IFN\gamma}$ a degradation term (13, 54). The production term of IFNγ depends on $CD4^+$ and $CD8^+$ T-cells according to a previous experimental study (21).

Furthermore, IFNγ affects the hydraulic permeability of the vessel wall, L_p. In the model, L_p is given as a function of the vessel wall pore size, r_o, the fraction of the vessel surface occupied by pores, γ, the viscosity of the fluid in the pores, η, and the thickness of the vessel wall, L_w:

$$L_p = \frac{\gamma r_0^2}{8\eta L_{vw}} \tag{28}$$

To account for the effect of IFNγ on vessel permeability, we incorporate experimental data showing that elimination of $CD4^+$ and $CD8^+$ T-cells leads to a decrease in IFNγ, which in turn increases vessel wall pore size and vessel permeability by 5-fold (21, 22).

Solution strategy

The model consists of a spherical tumor domain embedded at the center of a cubic host domain two orders of magnitude larger to avoid any boundary effects on the growth of the tumor; due to symmetry, only one eighth of the system was considered. To this end, Equations (1)-(28) were solved simultaneously using the commercial finite element software COMSOL Multiphysics (COMSOL, Inc., Burlington, MA, USA). Values for the model parameters are provided in Supplementary Table 1. The boundary conditions for the continuity of the stress and displacement fields, as well as the concentration of the oxygen at the interface between the tumor and the normal tissue, were applied automatically by the software, the remaining boundary conditions are shown in Supplementary Figure S6. The model consists of 655,458 degrees of freedom (109,341 finite elements) and it takes 23hr 46min 14 sec to simulate tumor growth for 30 days. The COMSOL code is available in (55).

References

1. Rodriguez EK, Hoger A, & McCulloch AD (1994) Stress-dependent finite growth in soft elastic tissues. *Journal of biomechanics* 27(4):455-467.
2. Skalak R, Zargaryan S, Jain RK, Netti PA, & Hoger A (1996) Compatibility and the genesis of residual stress by volumetric growth. *Journal of mathematical biology* 34(8):889-914.
3. Kim Y, Stolarska MA, & Othmer HG (2011) The role of the microenvironment in tumor growth and invasion. *Prog Biophys Mol Bio* 106(2):353-379.
4. Stylianopoulos T*, et al.* (2013) Coevolution of solid stress and interstitial fluid pressure in tumors during progression: implications for vascular collapse. *Cancer research* 73(13):3833-3841.
5. Roose T, Netti PA, Munn LL, Boucher Y, & Jain RK (2003) Solid stress generated by spheroid growth estimated using a linear poroelasticity model. *Microvasc Res* 66(3):204-212.
6. MacLaurin J, Chapman J, Jones GW, & Roose T (2012) The buckling of capillaries in solid tumours. *P Roy Soc a-Math Phy* 468(2148):4123-4145.
7. Voutouri C & Stylianopoulos T (2014) Evolution of osmotic pressure in solid tumors. *J Biomech*.
8. Mpekris F, Baish JW, Stylianopoulos T, & Jain RK (2017) Role of vascular normalization in benefit from metronomic chemotherapy. *Proceedings of the National Academy of Sciences of the United States of America* 114(8):1994-1999.
9. de Pillis LG, Radunskaya AE, & Wiseman CL (2005) A validated mathematical model of cell-mediated immune response to tumor growth. *Cancer research* 65(17):7950-7958.
10. Goldman A*, et al.* (2015) Temporally sequenced anticancer drugs overcome adaptive resistance by targeting a vulnerable chemotherapy-induced phenotypic transition. *Nature communications* 6:6139.
11. Conley SJ*, et al.* (2012) Antiangiogenic agents increase breast cancer stem cells via the generation of tumor hypoxia. *Proceedings of the National Academy of Sciences of the United States of America* 109(8):2784-2789.
12. Todaro M*, et al.* (2009) Efficient killing of human colon cancer stem cells by gammadelta T lymphocytes. *Journal of immunology* 182(11):7287-7296.
13. Mahlbacher G, Curtis LT, Lowengrub J, & Frieboes HB (2018) Mathematical modeling of tumor-associated macrophage interactions with the cancer microenvironment. *Journal for immunotherapy of cancer* 6(1):10.
14. Casciari JJ, Sotirchos SV, & Sutherland RM (1992b) Mathematical-Modeling of Microenvironment and Growth in Emt6/Ro Multicellular Tumor Spheroids. *Cell Proliferat* 25(1):1-22.
15. Casciari JJ, Sotirchos SV, & Sutherland RM (1992a) Variations in Tumor-Cell Growth-Rates and Metabolism with Oxygen Concentration, Glucose-Concentration, and Extracellular Ph. *J Cell Physiol* 151(2):386-394.
16. Fouchet D & Regoes R (2008) A population dynamics analysis of the interaction between adaptive regulatory T cells and antigen presenting cells. *PloS one* 3(5):e2306.
17. Burroughs NJ, Oliveira BMPM, Pinto AA, & Ferreira M (2011) Immune response dynamics. *Math Comput Model* 53(7-8):1410-1419.
18. Barsoum IB, Smallwood CA, Siemens DR, & Graham CH (2014) A mechanism of hypoxia-mediated escape from adaptive immunity in cancer cells. *Cancer research* 74(3):665-674.
19. Perelson AS, Kirschner DE, & De Boer R (1993) Dynamics of HIV infection of CD4+ T cells. *Mathematical biosciences* 114(1):81-125.
20. Culshaw RV & Ruan S (2000) A delay-differential equation model of HIV infection of CD4(+) T-cells. *Mathematical biosciences* 165(1):27-39.

21. Tian L*, et al.* (2017) Mutual regulation of tumour vessel normalization and immunostimulatory reprogramming. *Nature* 544(7649):250-254.
22. De Palma M & Jain RK (2017) CD4+ T Cell Activation and Vascular Normalization: Two Sides of the Same Coin? *Immunity* 46(5):773-775.
23. de Pillis L, Caldwell T, Sarapata E, & Williams H (2013) Mathematical Modeling of Regulatory T Cell Effects on Renal Cell Carcinoma Treatment. *Discrete Cont Dyn-B* 18(4):915-943.
24. Wang Q*, et al.* (2010) Reoxygenation of hypoxia-differentiated dentritic cells induces Th1 and Th17 cell differentiation. *Molecular immunology* 47(4):922-931.
25. Rolny C*, et al.* (2011) HRG inhibits tumor growth and metastasis by inducing macrophage polarization and vessel normalization through downregulation of PlGF. *Cancer cell* 19(1):31-44.
26. Hermann PC*, et al.* (2007) Distinct populations of cancer stem cells determine tumor growth and metastatic activity in human pancreatic cancer. *Cell stem cell* 1(3):313-323.
27. Milberg O*, et al.* (2019) A QSP Model for Predicting Clinical Responses to Monotherapy, Combination and Sequential Therapy Following CTLA-4, PD-1, and PD-L1 Checkpoint Blockade. *Scientific reports* 9(1):11286.
28. Huang Y, Snuderl M, & Jain RK (2011) Polarization of tumor-associated macrophages: a novel strategy for vascular normalization and antitumor immunity. *Cancer cell* 19(1):1-2.
29. Huang Y, Goel S, Duda DG, Fukumura D, & Jain RK (2013) Vascular normalization as an emerging strategy to enhance cancer immunotherapy. *Cancer research* 73(10):2943-2948.
30. Linde N*, et al.* (2012) Vascular endothelial growth factor-induced skin carcinogenesis depends on recruitment and alternative activation of macrophages. *The Journal of pathology* 227(1):17-28.
31. Stockmann C*, et al.* (2008) Deletion of vascular endothelial growth factor in myeloid cells accelerates tumorigenesis. *Nature* 456(7223):814-818.
32. Mow VC, Kuei SC, Lai WM, & Armstrong CG (1980) Biphasic Creep and Stress-Relaxation of Articular-Cartilage in Compression - Theory and Experiments. *J Biomech Eng-T Asme* 102(1):73-84.
33. Taber LA (2008) Theoretical study of Beloussov's hyper-restoration hypothesis for mechanical regulation of morphogenesis. *Biomechanics and modeling in mechanobiology* 7(6):427-441.
34. Ciarletta P (2013) Buckling Instability in Growing Tumor Spheroids. *Phys Rev Lett* 110(15).
35. Voutouri C, Mpekris F, Papageorgis P, Odysseos AD, & Stylianopoulos T (2014) Role of constitutive behavior and tumor-host mechanical interactions in the state of stress and growth of solid tumors. *PloS one* 9(8):e104717.
36. Xu G, Bayly PV, & Taber LA (2009) Residual stress in the adult mouse brain. *Biomechanics and modeling in mechanobiology* 8(4):253-262.
37. Xu G*, et al.* (2010) Opening angles and material properties of the early embryonic chick brain. *Journal of biomechanical engineering* 132(1):011005.
38. Griffon-Etienne G, Boucher Y, Brekken C, Suit HD, & Jain RK (1999) Taxane-induced apoptosis decompresses blood vessels and lowers interstitial fluid pressure in solid tumors: clinical implications. *Cancer research* 59(15):3776-3782.
39. Mpekris F, Angeli S, Pirentis AP, & Stylianopoulos T (2015) Stress-mediated progression of solid tumors: effect of mechanical stress on tissue oxygenation, cancer cell proliferation, and drug delivery. *Biomechanics and modeling in mechanobiology* 14(6):1391-1402.
40. Stylianopoulos T & Jain RK (2013) Combining two strategies to improve perfusion and drug delivery in solid tumors. *Proceedings of the National Academy of Sciences of the United States of America* 110((46)):18632-18637.
41. Popel AS (1989) Theory of oxygen transport to tissue. *Critical reviews in biomedical engineering* 17(3):257-321.

42. Chauhan VP, Stylianopoulos T, Boucher Y, & Jain RK (2011) Delivery of molecular and nanomedicine to tumors: Transport barriers and strategies. *Annual Reviews Chemical and Biomolecular Engineering* 2:281-298.
43. Schugart RC, Friedman A, Zhao R, & Sen CK (2008) Wound angiogenesis as a function of tissue oxygen tension: a mathematical model. *Proceedings of the National Academy of Sciences of the United States of America* 105(7):2628-2633.
44. Plank MJ, Sleeman BD, & Jones PF (2004) The role of the angiopoietins in tumour angiogenesis. *Growth factors* 22(1):1-11.
45. Boige V*, et al.* (2012) Efficacy, safety, and biomarkers of single-agent bevacizumab therapy in patients with advanced hepatocellular carcinoma. *The oncologist* 17(8):1063-1072.
46. Willett CG*, et al.* (2004) Direct evidence that the VEGF-specific antibody bevacizumab has antivascular effects in human rectal cancer. *Nat Med* 10(2):145-147.
47. Zheng XM, Koh GY, & Jackson T (2013) A Continuous Model of Angiogenesis: Initiation, Extension, and Maturation of New Blood Vessels Modulated by Vascular Endothelial Growth Factor, Angiopoietins, Platelet-Derived Growth Factor-B, and Pericytes. *Discrete Cont Dyn-B* 18(4):1109-1154.
48. Hutchinson LG*, et al.* (2016) Vascular phenotype identification and anti-angiogenic treatment recommendation: A pseudo-multiscale mathematical model of angiogenesis. *Journal of theoretical biology* 398:162-180.
49. Zagzag D*, et al.* (2006) Hypoxia-inducible factor 1 and VEGF upregulate CXCR4 in glioblastoma: implications for angiogenesis and glioma cell invasion. *Laboratory investigation; a journal of technical methods and pathology* 86(12):1221-1232.
50. Zheng X, Koh GY, & Jackson T (2013) A CONTINUOUS MODEL OF ANGIOGENESIS: INITIATION, EXTENSION, AND MATURATION OF NEW BLOOD VESSELS MODULATED BY VASCULAR ENDOTHELIAL GROWTH FACTOR, ANGIOPOIETINS, PLATELET-DERIVED GROWTH FACTOR-B, AND PERICYTES. *Discrete and continuous dynamical systems series B* 18(4):1109-1154.
51. Zheng X, Koh GY, & Jackson T (2013) A continuous model of angiogenesis: initiation, extension, and maturation of new blood vessels modulated by vascular endothelial growth factor, angiopoietins, platelet-derived growth factor-B, and pericytes. *Discrete & Continuous Dynamical Systems-B* 18(4):1109-1154.
52. Billy F*, et al.* (2009) A pharmacologically based multiscale mathematical model of angiogenesis and its use in investigating the efficacy of a new cancer treatment strategy. *Journal of theoretical biology* 260(4):545-562.
53. Gevertz JL & Torquato S (2006) Modeling the effects of vasculature evolution on early brain tumor growth. *Journal of theoretical biology* 243(4):517-531.
54. Rateitschak K*, et al.* (2010) Mathematical modelling of interferon-gamma signalling in pancreatic stellate cells reflects and predicts the dynamics of STAT1 pathway activity. *Cellular signalling* 22(1):97-105.
55. Mpekris F*, et al.* (2020) COMSOL code. *Zenodo* https://zenodo.org/record/3611065#.XiHj-MgzaMo(17/01/2020).
56. Netti PA, Berk DA, Swartz MA, Grodzinsky AJ, & Jain RK (2000) Role of extracellular matrix assembly in interstitial transport in solid tumors. *Cancer Res* 60(9):2497-2503.
57. Tracqui P (1995) From passive diffusion to active cellular migration in mathematical models of tumour invasion. *Acta biotheoretica* 43(4):443-464.
58. Voutouri C*, et al.* (2019) Experimental and computational analyses reveal dynamics of tumor vessel cooption and optimal treatment strategies. *Proceedings of the National Academy of Sciences of the United States of America* 116(7):2662-2671.

59. Huang Y*, et al.* (2012) Vascular normalizing doses of antiangiogenic treatment reprogram the immunosuppressive tumor microenvironment and enhance immunotherapy. *Proceedings of the National Academy of Sciences of the United States of America* 109(43):17561-17566.
60. Zheng X*, et al.* (2018) Increased vessel perfusion predicts the efficacy of immune checkpoint blockade. *The Journal of clinical investigation* 128(5):2104-2115.
61. Chauhan VP*, et al.* (2019) Reprogramming the microenvironment with tumor-selective angiotensin blockers enhances cancer immunotherapy. *Proceedings of the National Academy of Sciences of the United States of America* 116(22):10674-10680.
62. Chen IX*, et al.* (2019) Blocking CXCR4 alleviates desmoplasia, increases T-lymphocyte infiltration, and improves immunotherapy in metastatic breast cancer. *Proceedings of the National Academy of Sciences of the United States of America* 116(10):4558-4566.
63. Shigeta K*, et al.* (2019) Dual PD-1 and VEGFR-2 blockade promotes vascular normalization and enhances anti-tumor immune responses in HCC. *Hepatology* doi: 10.1002/hep.30889.

Table S1 Parameter values used in the model

Parameter	Description	Value	Reference
k_{th}	hydraulic conductivity	6.5×10^{-10} $m^2\cdot Pa^{-1}\cdot day^{-1}$	(56)
C_{iox}	initial oxygen concentration	0.2 $mol\cdot m^{-3}$	(8)
D_{ox}	oxygen diffusion coefficient	1.55×10^{-4} $m^2\cdot day^{-1}$	(3)
A_{ox}	oxygen uptake	2,200 $mol\cdot m^{-3}\cdot day^{-1}$	(3, 15)
k_{ox}	oxygen uptake	0.00464 $mol\cdot m^{-3}$	(3, 15)
k_1	growth rate parameter	3,50 day^{-1}	---
k_2	growth rate parameter	0.0083 $mol\cdot m^{-3}$	(15)
a_{csc}	stem-cell-like cell growth multiplier	range **: 1-2 [-]	(17)
a_I	induced cancer cell growth multiplier	range **: 1-2 [-]	---
c	fractional tumor cell kill by NK cells	range *: 3.23×10^{-7} - 3.23×10^{-6} $cell^{-1}\cdot day^{-1}$	(9)
d_{im}	fractional tumor cell kill by $CD8^+$ T-cells	range *: 1.43 – 7.15 day^{-1}	(9)
λ_{im}	exponent of fractional cell kill by $CD8^+$ T-cells	1.36 [-]	(9)
s	steepness coefficient of the tumor-$CD8^+$ T-cells competition term	2.73 [-]	(9)
σ_{nk}	constant source of NK cells	1.3×10^4 $cells\cdot day^{-1}$	(9)
f_{Nk}	death rate of NK cells	range **: 0.0412 - 0.0814 day^{-1}	(9)

m_{T8}	death rate of $CD8^+$ T-cells	range **: 0.02 - 0.04 day^{-1}	(9)
m_{reg}	death rate of regulatory T-cells	0.02 day^{-1}	(16)
g_{NK}	recruitment rate of NK cells	0.025 day^{-1}	(9)
j_{T8}	recruitment rate of $CD8^+$ T-cells	0.0375 day^{-1}	(9)
g_{reg}	recruitment rate of regulatory T-cells	0.0375 day^{-1}	(16)
h	steepness coefficient of NK cell recruitment curve	2.02×10^7 $cell^2$	(9)
p_{im}	inactivation rate of NK cells	1×10^{-7} $cell^{-1}\cdot day^{-1}$	(9)
k_{im}	steepness coefficient of $CD8^+$ T-cells recruitment curve	2.02×10^7 $cell^2$	(9)
q	inactivation rate of $CD8^+$ T-cells	3.42×10^{-10} $cell^{-1}\cdot day^{-1}$	(9)
r	stimulation rate of $CD8^+$ T-cells	1.1×10^{-7} $cell^{-1}\cdot day^{-1}$	(9)
λ_{reg}	inhibition term of NK cells and $CD8^+$ T-cells from Treg cells	100 $cell^{-1}\cdot day^{-1}$	(16)
p_{TC}	rate of dedifferentiation from cancer cells to stem-like-cell cancer cells	0.55 day^{-1}	(10)

p_{CT}	rate of transition from stem-like-cell cancer cells to cancer cells	1 day^{-1}	(10)
p_{CI}	rate of transition from stem-like-cell cancer cells to induced cancer cells	0.58 day^{-1}	(10)
p_{IC}	rate of transition from induced cancer cells to stem-like-cell cancer cells	0.96 day^{-1}	(10)
p_{TI}	rate of transition from cancer cells to induced cancer cells	0.21 day^{-1}	(10)
p_{IT}	rate of transition from induced cancer cells to cancer cells	1 day^{-1}	(10)
D_{VEGF}	VEGF diffusion coefficient	$3.1x10^{-11}$ [m^2/s]	(43)
D_{ec}	Endothelial cell diffusion coefficient	$1x10^{-15}$ [m^2/s]	(44)
D_{cell}	Cell diffusion coefficient	$1.5x10^{-11}$ [m^2/s]	(57, 58)
D_{pb}	PDGF-B diffusion coefficient	$1.65x10^{-3}$ [mm^2/h]	(48)
β_{pb}	Non-negative parameter	$1.25x10^{4}$ [1/h]	(48)
γ_{pb}	Non-negative parameter	$2.5x10^{6}$ [1/(μM.h]	(48)

μ_{pb}	Non-negative parameter	10^{-1} [1/h]	(48)
λ_{pb}	Positive parameter	100%	(48)
c_{pb}	Positive parameter	$3.33\text{x}10^{-3}$ [μM]	(48)
D_{pc}	Diffusion coefficient of motile pericyte	$1.65\text{x}10^{-3}$ [mm^2/h]	(48)
k_{pc}	Pericyte chemotactic	10^{-1} [mm^2/(μM.h)]	(48)
β_{pc}	Non-negative parameter	$1.25\text{x}10^{-1}$ [1/h]	(48)
μ_{pc}	Non-negative parameter	$4.17\text{x}10^{-2}$ [1/h]	(48)
μ_{pc2}	Non-negative parameter	$4.17\text{x}10^{-2}$ [1/h]	(48)
a_{pc1}	Positive parameter	$3.33\text{x}10^{-3}$ [μM]	(48)
a_{pc2}	Positive parameter	10^{-3} [μM]	(48)
a_{pc3}	Positive parameter	10^{-3} [μM]	(48)
a_{pc4}	Positive parameter	$4.17\text{x}10^{-3}$ [1/h]	(48)
p_c^0	Reference pericyte	$3.32\text{x}10^{-8}$ [μM]	(48)
x_n	Chemotactic endothelial cell	$2\text{x}10^{-15}$ [m^5/kg-s]	(43)
W_{ST}	Weight between oxygen- CXCL12	1	(43)
W_{Se}	Weight between VEGF- CXCL12	1	(43)
C_s^0	Reference CXCL12 concentration	$1\text{x}10^{-3}$ [g/m^3]	(43)
C_{vegf}^0	Reference VEGF concentration	$1\text{x}10^{-3}$ [g/cm^3]	(43)
e^0	Reference value of endothelial cell	$1\text{x}10^{-3}$ [g/cm^3]	(43)

a_1^0	Reference a_1 concentration	$1x10^{-3}$ [g/cm^3]	(44)
a_2^0	Reference a_2 concentration	$1x10^{-3}$ [g/cm^3]	(44)
λ_1	Positive parameters	$1x10^{-3}$ [cm^3/g-s]	(43)
λ_2	Positive parameters	$1x10^{-5}$ [cm^3/g-s]	(43)
λ_3	Positive parameters	$1x10^{-3}$ [cm^3/g-s]	(43)
λ_4	Positive parameters	$1x10^{-1}$ [cm^3/g-s]	(43)
λ_5	Positive parameters	$5.56x10^{-7}$[1/s]	(43)
λ_{10}	Positive parameters	$6.8x10^{-3}$ [1/s]	(43)
λ_{11}	Positive parameters	4 [cm^3/g-s]	(43)
λ_{12}	Positive parameters	4 [cm^3/g-s]	(43)
λ_{13}	Positive parameters	$4x10^{-5}$ [1/s]	(43)
b_1	Positive parameters	2280 [1/h]	(44)
b_2	Positive parameters	18240 [1/h]	(44)
μ_1	Positive parameters	456 [1/h]	(44)
μ_2	Positive parameters	456 [1/h]	(44)
s_1	Positive parameters	$1x10^3$ [cm^3/ g]	(44)
s_2	Positive parameters	$1x10^3$ [cm^3/ g]	(44)
λ_{M1}	tumoricidal effect of M1-like TAMs in cancer cells	3 s^{-1}	(13)
s_{CD4}	source term of $CD4^+$ T-cells	150 day^{-1}**	(19)
μ_{Cd4}	natural death rate of $CD4^+$ T-cells	0.02 day^{-1}	(19)
re_{Cd4}	the growth rate of $CD4^+$ T-cells	0.03 day^{-1}	(19)

r_{Cd4}	stimulation rate of $CD8^+$ T cells by $CD4^+$ T-cells	$1x10^{-15}$ $cells^{-1}.day^{-1}$	(23)
σ_{T8}	source term of $CD8^+$ T-cells	150 day^{-1}	----
m_{M1}	death rate of regulatory M1-like TAMs	0.02 day^{-1}	----
m_{M2}	death rate of regulatory M2-like TAMs	0.02 day^{-1}	----

*: linear increase from minimum to maximum value depending on oxygen levels

**: linear decrease from maximum to minimum value depending on oxygen levels

Table S2 Value of parameter k_1 used for fitting the model to experimental data

Experimental study	k_1
Huang et. al. (59)	2.06 day^{-1}
Zheng et. al. (60)	1.84 day^{-1}
Chauhan et. al. (61)	2.30 day^{-1} (E0771) 2.35 day^{-1} (MCa-MC3)
Chen et. al. (62)	2.00 day^{-1}
Shigeta et. al. (63)	2.10 day^{-1}

Table S3 Association of treatment strategies with mathematical model's parameters

Treatment	Model parameter variation
Vascular normalization	Increase in the endothelial cells and VEGF degradation rate constants (parameters k_{a-vegf}^{ec} and k_{a-vegf}^{vegf} in Supplementary Eqs. 19 and 22 respectively)
Stroma normalization	Decrease in the mechanical properties of the tumor (parameters μ and k in Supplementary Eq. 16)
Immunotherapy	Increase in the source term of $CD8^+$ T cells (parameter σ_{T8} in Supplementary Eq. 8) for anti-PD-1 and increase of the death rate of Treg cells for anti-CTLA-4 (parameter m_{reg} in Supplementary Eq. 8)

Figure S1 Phase diagram for the effect of different doses of anti-VEGF treatment combined with different values of the source term of $CD8^+$ T-cells to model immunotherapy for sequential administration on (**A**) Stem-like cancer cells and (**B**) Induced cancer cells. We observe that both low and high doses of anti-VEGF treatment in combination with highest values of immunotherapy are effective but for lower values of immunotherapy only low doses of anti-VEGF treatment decrease number of cells. The values of the model parameters presented in the figure were calculated halfway between the tumor center and periphery.

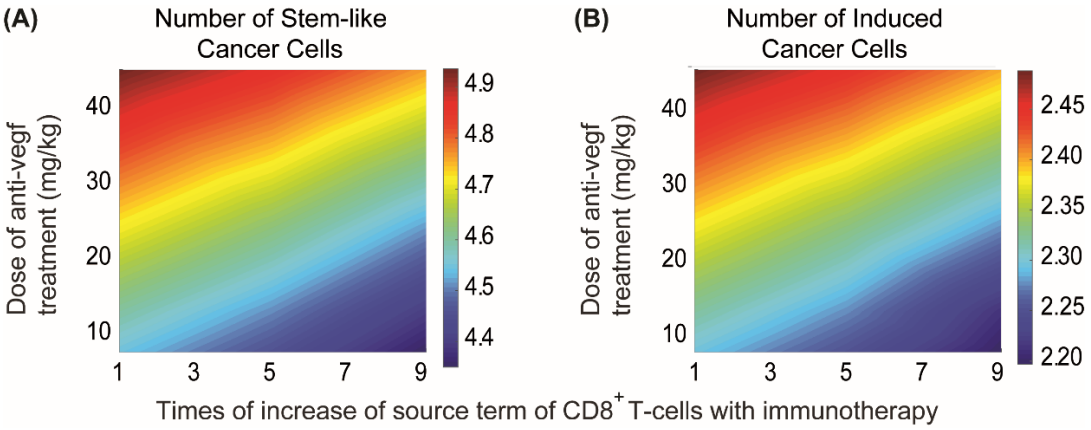

Figure S2 Effect of different values of the tumor elastic modulus combined with different values of the source term of $CD8^+$ T-cells to model the immunotherapy for sequential administration. (A)-(I) Phase diagrams for the effect of combinatorial treatment of stroma normalization with immunotherapy on functional vascular density, tumor oxygenation, VEGF levels, effector immune cells (NK and $CD8^+$ T-cells) and $CD4^+$ T-cells, M1-like and M2-like TAMs, cancer cell population and tumor volume. Values of model parameters presented in the figure were calculated halfway between the tumor center and periphery.

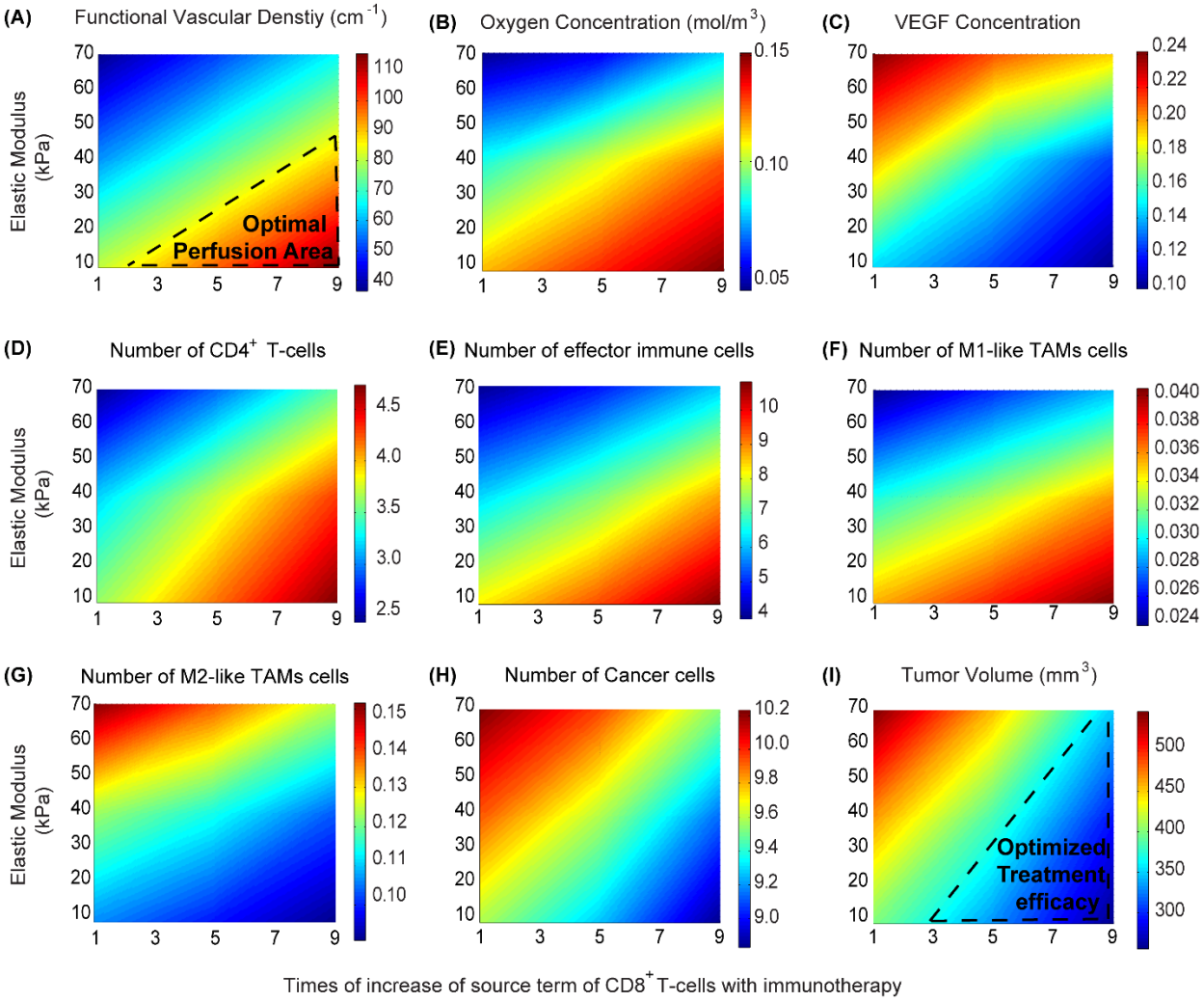

Figure S3 Phase diagram for the effect of different values of elastic modulus combined with different values of the source term of $CD8^+$ T-cells to model immunotherapy on (**A**) Stem-like cancer cells and (**B**) Induced cancer cells. We observe that decrease of Elastic Modulus and alleviation of solid stress enhance the efficacy of immunotherapy. The values of the model parameters presented in the figure were calculated halfway between the tumor center and periphery.

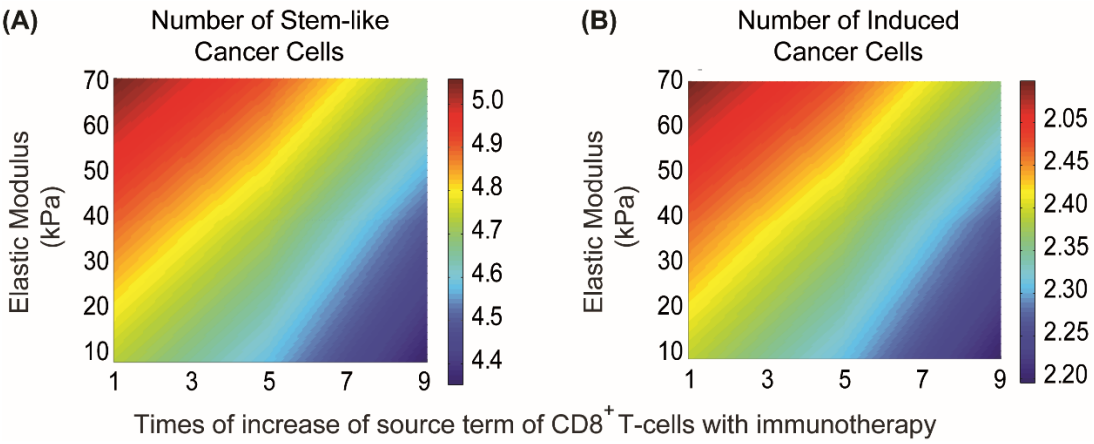

Figure S4 Effect of simultaneous triple therapy of vascular and stroma normalization combined with immunotherpy on tumor volume. Triple therapy is more effective compared to the combinatorial treatment of immunotherapy with vascular normalization or stroma normalization.

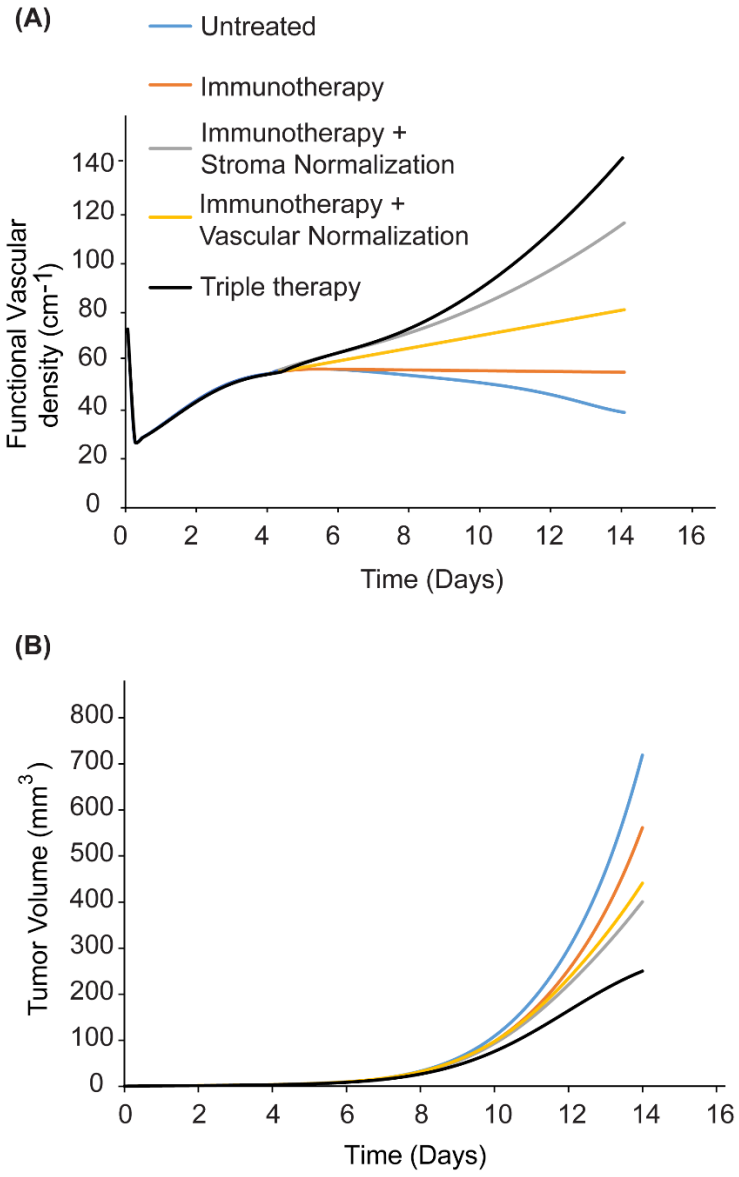

Figure S5 Phase digrams of overall tumor volume for the effect of different proliferation and migration (i.e. diffussion) rates of cancer cells in sequential administration of anti-VEGF treatment and immunotherapy. The values of proliferation rates varied from 2.20 to 2.40 day^{-1} and the values of the diffusion coefficient varied from 1.5×10^{-11} to 1.5×10^{-13} (m^2/s). There is no significant difference between different doses of anti-VEGF treatment in overall tumor volume. On the other hand, increasing proliferation and migration rates, the lower values of anti-VEGF treatment are more effective. Furthermore, the differences between anti-VEGF doses are are more sensitive to changes in the proliferation rate of cancer cells than their migration rate.

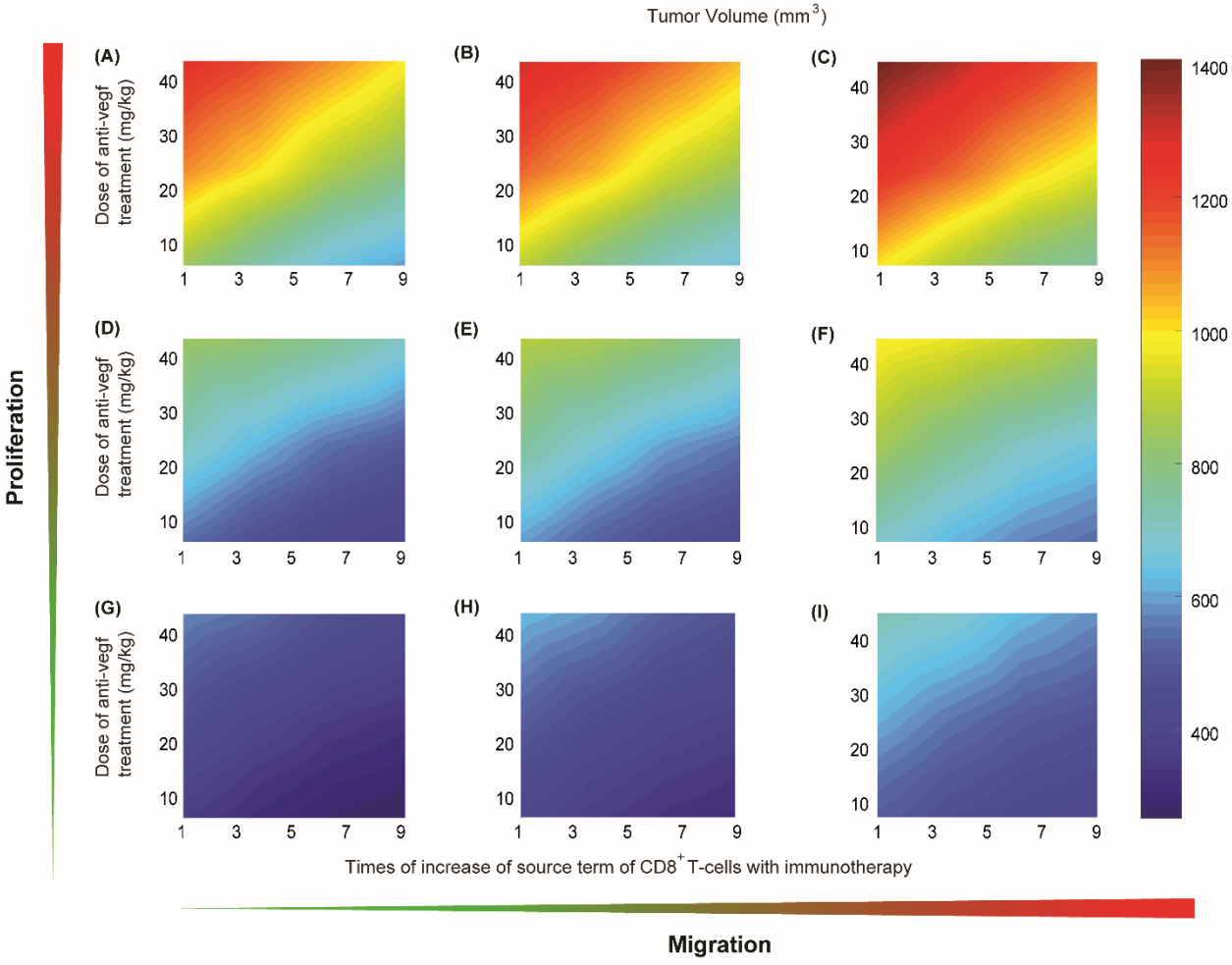

Figure S6 Computational domain and boundary conditions employed.